

Low-Resistance Hole Contact Stacks for Interdigitated Rear-Contact Silicon Heterojunction Solar Cells

Philipp Wagner, Alexandros Cruz, Johann-Christoph Stang, and Lars Korte

Abstract— Achieving low contact resistivity for the p-contact in silicon heterojunction (SHJ) solar cells is challenging when classic n-type transparent conductive oxides (TCOs), such as indium tin oxide (ITO), are used in the contact stack. Here, we report on SHJ solar cells with interdigitated back-contact (IBC) and a direct aluminium (Al) metallisation applied to the p-contact. We find that carefully annealing an Al/a-Si:H(p) (p-type amorphous silicon) contact at moderate temperatures leads to a specific contact resistivity that is half as low as its silver (Ag)/ITO counterpart. This is explained by Al diffusing into a-Si:H(p) upon temperature treatment, forming a partially crystallised aluminium silicide layer. For a sufficiently high doping level in a-Si:H(p), this enables an efficient tunnel-recombination of holes from a-Si:H(p) to the Al contact. An estimate for this tunnelling-dominated specific contact resistivity is calculated as a function of the interface doping density. Best fabricated IBC SHJ solar cells with Al p-contact yield a fill factor of 77.5% and a power conversion efficiency of 22.3%. The main differences to devices with an Ag/ITO/a-Si:H(p) contact stack are a decrease in open-circuit voltage by 14 mV and a slightly higher series resistance (R_s). While the first aspect can be ascribed to increased interface recombination, the second one is unexpected and requires further investigation. Interestingly, omitting an intermediate TCO does not lead to current losses in devices with Al contacts, which is further investigated by optical simulations. Finally, electrical equivalent circuit simulations are conducted to describe the electrical behaviour of the investigated devices.

Index Terms—Aluminium metallisation, electrical equivalent circuit simulation, interdigitated back-contact (IBC) solar cells, silicon heterojunction (SHJ) solar cells, specific contact resistivity, transfer-length method (TLM), optical simulation

I. INTRODUCTION

PASSIVATED contacts in solar cell applications have enabled outstanding device performance especially in

Manuscript received ...; revised ...; accepted This work was supported in part by the HZB institute EMIL and the HySPRINT Helmholtz Innovation Lab.

Philipp Wagner and Lars Korte are with the Young Investigator Group Perovskite Tandem Solar Cells, Helmholtz Zentrum Berlin für Materialien und Energie GmbH, 12489 Berlin, Germany (emails: philipp.wagner@helmholtz-berlin.de; korte@helmholtz-berlin.de).

Alexandros Cruz is with the PVcomB, Helmholtz Zentrum Berlin für Materialien und Energie GmbH, 12489 Berlin, Germany (email: alexandros.cruz@helmholtz-berlin.de).

Johann-Christoph Stang was with the Institute of Silicon Photovoltaics, Helmholtz Zentrum Berlin für Materialien und Energie GmbH, 12489 Berlin, Germany. He is currently available under his private email address (email: cjs@live.de).

terms of achieving open-circuit voltages (V_{oc} s) as high as 750 mV [1]. In this regard, undoped (nominally intrinsic) hydrogenated amorphous silicon, a-Si:H(i), provides excellent chemical surface passivation by means of saturation of dangling silicon bonds [2]. Applying a rear-contact scheme to this silicon heterojunction (SHJ) architecture and thereby eliminating shading losses at the device's front side has led to the currently most successful approach in silicon wafer-based solar cell technology with a power conversion efficiency (PCE) as high as 26.7% [3],[4]. However, complex contact preparation, usually relying on techniques such as photolithography, which are not applicable to industrial fabrication, is a major drawback of this approach. Photolithography-free fabrication routes have therefore been pursued by several groups [5]–[12] with the tunnel-junction IBC (interdigitated back-contact) [12] being currently the most successful and potentially the most industrially viable option. An ongoing and as of yet unsolved matter in these devices both for rear-contacted and standard SHJ solar cells is, however, the inequality in specific contact resistivity (ρ_c) of differently doped contacts. Here, the p-contact's ρ_c exceeds by far that of the n-contact when a standard silver/indium tin oxide (Ag/ITO) contact stack is used [13]. This partly stems from the choice of material. Conventionally, n-type transparent conductive oxides (TCOs) are used for both contacts [14]. This is due to low hole mobilities of most p-type TCOs [15] and insufficient air stability [16]. Additionally, it is challenging to achieve high doping levels in p-type TCOs due to hole compensation [17]. The configuration of n-type TCO and p-type a-Si:H necessitates high doping concentrations at least at their interface in order to allow for effective charge carrier extraction by means of inter-band tunnelling [18],[19]. Replacing Ag/TCO with diffused aluminium (Al) is an interesting approach both in terms of contact engineering and in the context of industrialisation: Ag and ITO have been identified as a major cost-driver in SHJ technology [20]. Aluminium, just like boron, is a p-type dopant and, being a highly conductive metal as well, is suitable for forming a lowly resistive ohmic contact with a-Si:H(p) [21],[22], provided that the doping concentration in a-Si:H(p) is sufficiently high [18],[23],[24]. In fact, ρ_c s as low as $1 \text{ m}\Omega\text{cm}^2$ have been reported for contacts consisting of Al interdiffused a-Si:H layers with surface doping concentrations of up to $5 \times 10^{19} \text{ cm}^{-3}$ and film thicknesses ranging from

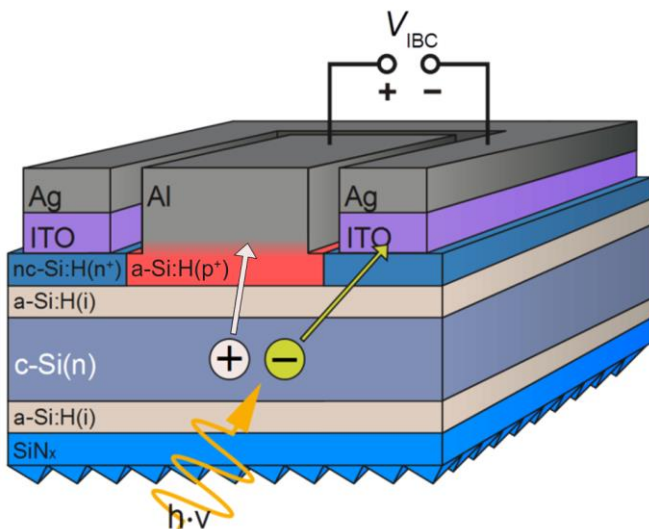


Fig. 1. Schematic of a silicon heterojunction solar cell with an interdigitated back-contact (not to scale). The rear side of the cell is facing up. The minority (p) and majority (n) charge carrier contact metallisation consist of diffused aluminium (illustrated by a colour gradient) and a silver/indium tin oxide stack respectively.

160–300 nm [21],[22],[25]; for diffused p-contacts passivated with 5–10 nm a-Si:H(i), specific contact resistivities were found to be as low as $100 \text{ m}\Omega\text{cm}^2$ [26]. However, Al is not an ideal choice for the metallisation of n-type nanocrystalline silicon because it leads to counterdoping upon interdiffusion [22]. Therefore, we propose a different metallisation approach here where Ag/ITO is replaced by diffused Al and Ag/ITO is kept for the n-contact. A schematic of the thus prepared solar cells is depicted in Fig. 1. This approach is based on our earlier works where IBC SHJ solar cells with an all-Al metallisation scheme have been investigated [27]. There, contact formation between a-Si:H(p) and Al has been explained by interdiffusion at moderate annealing temperatures and partial crystallisation of the thus formed aluminium silicide (Al_xSi_y) layer. It was further found that the final devices' FFs and V_{oc} s strongly correlate with the areal density of aluminium silicide crystallites formed in the a-Si:H during the annealing step. As a result, final devices feature either high FFs but low V_{oc} s or vice versa, but achieving high values for both parameters remains challenging because the demands for low contact resistivity (conductive but recombination-active Al spiking areas) and high V_{oc} s (areas with intact surface passivation) are difficult to reconcile. In the following we will present a possible mitigation to this dilemma by confining Al-related recombination losses to the p-contact.

II. EXPERIMENTAL

IBC SHJ solar cells are processed on $280 \mu\text{m}$ thick, 4", $1\text{--}5 \Omega\text{cm}$ float-zone wafers with polished rear and random pyramid textured front side. Following a standard cleaning procedure (RCA clean) and a 3 min dip in diluted 1% hydrofluoric acid (HF), intrinsic and doped amorphous (a-Si:H) and nanocrystalline (nc-Si:H) layers are deposited by means of plasma-enhanced chemical vapour deposition

(PECVD) in a semi-industrial AKT1600 cluster tool manufactured by Applied Materials operating at 13.56 MHz. A front side anti-reflective coating (ARC) consisting of 70 nm silicon nitride (SiN_x) is deposited in the same way. For further details regarding PECVD processes that are conducted at this tool, cf. [28]. ITO is deposited by RF sputtering in a tool manufactured by Roth & Rau. Ag and Al are thermally evaporated by using a Creamat 350 tool manufactured by CREAVAC. All rear-side layers are patterned by means of photolithography. In order to extract the ρ_c of different contact stacks, TLM (transfer-length method) [29] test samples are prepared on quarters of both p and n-type 4" double-side polished $1\text{--}5 \Omega\text{cm}$ float-zone wafer. The contact pads are also structured by photolithography. The dimensions of these contact pads are $1 \text{ cm} \times 0.05 \text{ cm}$, and the pad spacings are between 1 and 0.05 mm. To account for Al diffusion into the doped a-Si:H and to prevent penetration of the passivation layer upon annealing, doped layers used to investigate the Al contact are deposited with twice the thickness (18 instead of 9 nm) as underneath the standard Ag/ITO contact. For TLM measurements, samples are successively annealed at $160\text{--}190 \text{ }^\circ\text{C}$ (Al) or $200 \text{ }^\circ\text{C}$ (Ag/ITO) in increments of 5–10 min. TLM is remeasured and photoluminescence (PL) images are taken after each annealing step in order to investigate the change in ρ_c of different contact schemes and doping types, and to verify whether the passivation is still intact. After each process step during solar cell fabrication, PL imaging is used along with transient photoconductance decay (TrPCD) measurements [30]. All TrPCD measurements are carried out using a Sinton WCT-100 setup in transient mode. The same setup is used for measuring illumination intensity-dependent current–voltage characteristics (SunsVoc) after finished device fabrication [31]. Current density–voltage ($j\text{--}V$) characteristics are obtained under standard test conditions using a class AAA sun simulator with a tungsten and a xenon lamp (Wacom WXS-156S-L2). The designated illumination area [4] of $1 \text{ cm} \times 1 \text{ cm}$ is defined by a shadow mask applied to the front side. The external quantum efficiency (EQE) is measured for wavelengths from 300–1200 nm (10 nm increment) with a home built EQE setup featuring a spot size of $2 \text{ mm} \times 5 \text{ mm}$ and halogen and xenon lamps as illumination sources. Reflection measurements are conducted for wavelengths from 300 nm to 1200 nm (2 nm increment) using a Perkin Elmer LAMBDA 1050 UV/vis spectrometer with integrating sphere. Electrical equivalent circuit simulations are carried out with the numerical modelling tool LTspice [32].

III. RESULTS AND DISCUSSION

A. TLM Study

In order to gather quantitative data for the specific contact resistivity of different contact schemes, a comprehensive TLM study is conducted. Here, the p-contact is of particular interest because its contact resistivity holds by far the greatest share of the total series resistance (R_s) in SHJ solar cell both in standard and in IBC configuration [8],[12],[13],[33],[34].

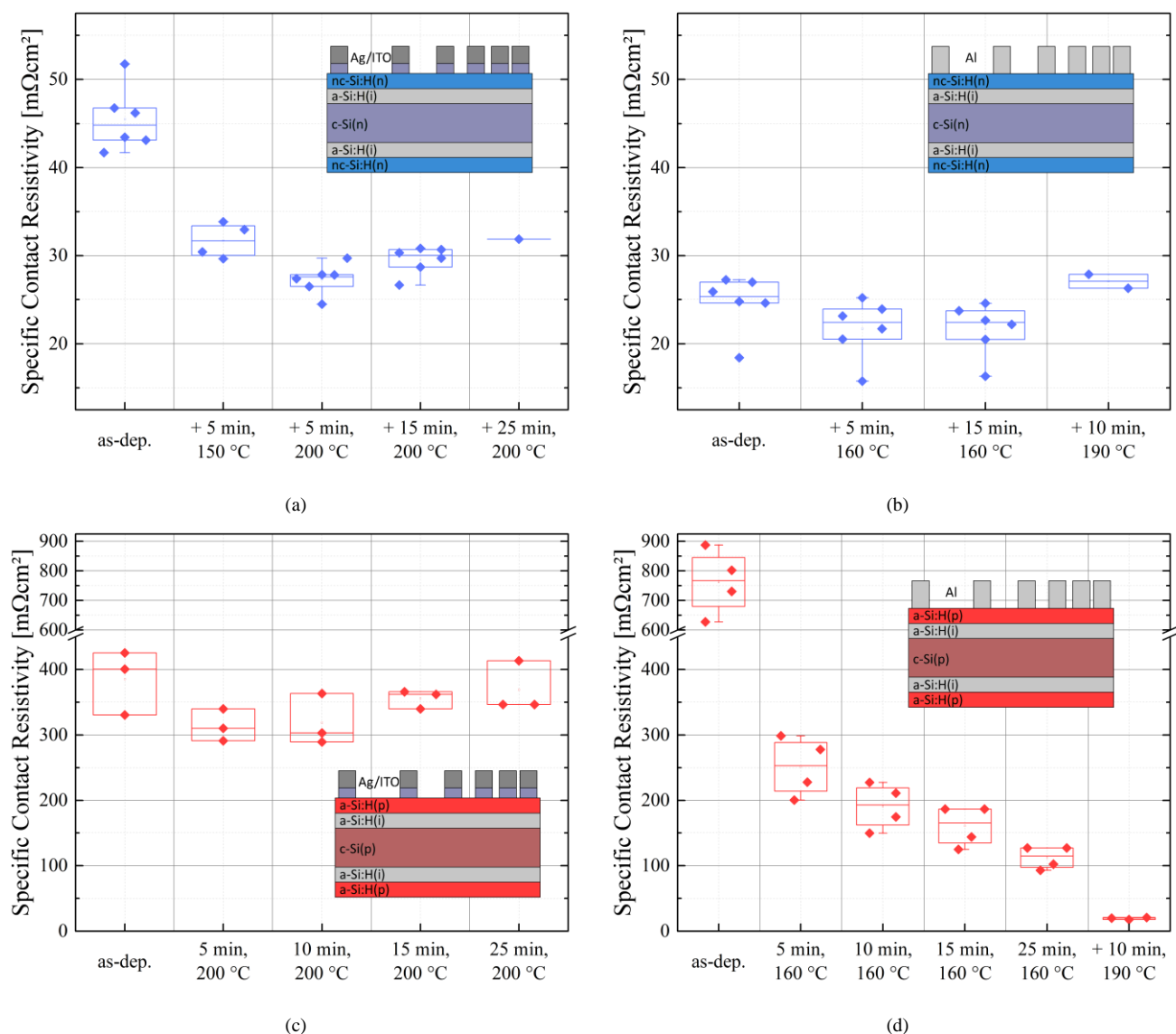


Fig. 2. Specific contact resistivity of (a) Ag/ITO on nc-Si:H(n), (b) Al on nc-Si:H(n), (c) Ag/ITO on a-Si:H(p), and (d) Al on a-Si:H(p) after different temperature treatment steps. Insets show a schematic (not to scale) of each investigated contact stack.

However, directly measuring the p-contact's ρ_c on a substrate with opposite polarity (here: n-type) is not possible as this forms a blocking junction (i.e. rectifying contact) whereas TLM measurements require ohmic contacts [12],[35]. Therefore, the fabrication of a TLM structure on a suitable substrate with otherwise identical contact stack (as on the final device) is necessary. It has been pointed out by LACHENAL *et al.* that the ρ_c extracted by TLM critically depends on the wafer's specific resistivity, which should be chosen according to the excess minority charge carrier density (Δn) in the final cell at maximum-power point (MPP) [12]. However, Δn_{MPP} is unknown before device fabrication as it depends on the quality of surface passivation. Therefore, p-type wafers with a specific wafer resistivity of 1–5 Ωcm (like their n-type counterparts) are used here, which allows for an insightful comparative TLM study, investigating the relative differences of the examined p-contact stacks.

In Fig. 2a–d, the resulting change of ρ_c upon annealing for

different contact schemes and doping types is depicted. After annealing the standard Ag/ITO/nc-Si:H(n) contact stack for 5 min at 150 °C, a substantial drop in ρ_c is observed (Fig. 2a). After another 5 min at 200 °C, a minimum value of 25–30 $\text{m}\Omega\text{cm}^2$ is attained, cutting the initial value nearly in half. This initial improvement is most probably due to hydrogen diffusion from the thin-film silicon layers to the TCO upon annealing and thereby slightly increasing the TCO's doping concentration at the ITO/nc-Si:H(n) interface. This mechanism has already been described by several authors [36]–[38]. Another important aspect, apart from this ρ_c improvement, that will (after device finalisation) positively affect the obtained FF is curing of sputter-induced damage to a-Si:H(i) during ITO deposition [39] by means of hydrogen redistribution within the passivation layer [40]. This second aspect applies to all investigated contact schemes and polarities that include ITO. The obtained minimum is also in line with previous findings in literature with a comparable

contact stack [13],[33],[41]. Further annealing leads again to a slight increase in ρ_c which is in accordance with recent literature but not understood yet [42]. Regarding the alternative diffused Al/nc-Si:H(n) contact stack, a fairly low ρ_c of about $25 \text{ m}\Omega\text{cm}^2$ is achieved after deposition and it improves only marginally upon annealing (Fig. 2b). This can be explained as follows: aluminium silicide has been reported to form already in as-deposited films on a-Si:H [43]. Temperatures of slightly above $100 \text{ }^\circ\text{C}$, which the substrates experience during deposition of Al, are already sufficient to cause a small decrease in ρ_c due to crystallisation of the interdiffused aluminium silicide layer. Apart from that, here, nanocrystalline silicon is used to form the n-contact. Its superior conductivity as compared to a-Si:H also results in a lower ρ_c [44]. It is further helpful that the work function of Al (4.3 eV) and electron affinity of amorphous silicon (3.9 eV) line up quite well and induce only a minor energetic barrier for electron extraction that can be overcome by thermionic emission. For ITO, a work function of 4.4–4.5 eV [45] has been reported, which leads to a slightly larger band offset between ITO and nc-Si:H(n) and therefore further explains the slightly lower ρ_c of an Al/nc-Si:H(n) contact. Extended annealing at higher temperatures ($190 \text{ }^\circ\text{C}$) increases the ρ_c , which is interpreted here as the onset of counterdoping [22]. In Fig. 2c, the standard Ag/ITO/a-Si:H(p) contact shows a qualitatively similar behaviour to its n-counterpart. The initial improvement is, again, most likely due to hydrogen diffusion from amorphous silicon to ITO (cf. above). The increase in ρ_c for prolonged annealing is probably due to hydrogen effusion from a-Si:H(i) [46]. This degradation occurs because an overlying boron doped film shifts the Fermi level in a-Si:H(i) towards its valence-band edge, thereby lowering the energy necessary to break Si–H bonds. As a result, temperatures well below $200 \text{ }^\circ\text{C}$ already suffice to degrade surface passivation in an a-Si:H(p/i) layer stack. The resulting poor surface passivation (due to increased surface recombination) is linked to a reduced FF as less charge carriers are extracted [47],[48]. The as-deposited Al/a-Si:H(p) contact's ρ_c is about twice as high ($> 800 \text{ m}\Omega\text{cm}^2$) as its Ag/ITO/a-Si:H(p) counterpart (Fig. 2d). In [43], it has been reported that non-diffused Al forms a rectifying Schottky contact with a-Si:H(p). In our case (since we are able to measure contact resistivity with this structure), the contact seems to be not fully rectifying, but rather features a very high contact resistivity. Furthermore, either there is no aluminium silicide formation already during Al deposition on a-Si:H(p) (the reported formation according to [43] were found for intrinsic layers), or the as-deposited contact resistivity is much higher because lowly conductive amorphous instead of nanocrystalline material is used. In addition, an unfavourable band alignment between Al and a-Si:H(p) leads to a large energetic barrier for holes that can only be overcome by band-to-band tunnelling, which appears not to be functional in the as-deposited state (in comparison: for an as-deposited Ag/ITO/a-Si:H(p) contact, tunnelling is also the predominant extraction mechanism and seems to be already functional due to a higher work function of ITO). This will be elaborated on in far greater detail in section D.

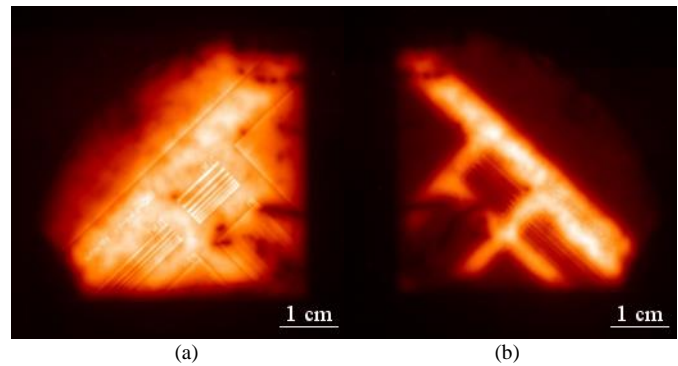


Fig. 3. Photoluminescence images of TLM test samples with diffused aluminium minority charge carrier contact stack. The images are taken with the metallisation on the wafer's rear side. (a) carefully annealing at moderate temperatures (15 min at $160 \text{ }^\circ\text{C}$, cf. Fig. 2d) leads to low specific contact resistivities and an intact surface passivation (bright areas) at the same time. (b) Elevated temperatures and/or long annealing durations (here: 25 min at $160 \text{ }^\circ\text{C}$ + 10 min at $190 \text{ }^\circ\text{C}$, cf. Fig. 2d) lead to aluminium completely penetrating the a-Si:H(i) layer, thereby damaging the surface passivation (dark areas).

However, annealing leads to a drastic decrease in ρ_c as Al starts to diffuse into a-Si:H(p) and initialises its partial crystallisation [26]. This is in good agreement with our earlier results [27] where careful annealing of Al contacted doped a-Si:H layers has led to an increased FF due to a decrease in ρ_c . This has been linked to the interaction of Al and a-Si:H (partially crystallised aluminium silicide layer), and the current transport mechanism is described as a combination of tunnelling (from a-Si:H to Al through a very thin silicide layer) and local current paths with high conductivity due to Al spiking through the a-Si:H layer stack. Here, a minimum ρ_c of only one tenth of what is achieved with an Ag/ITO metallisation is obtained. However, this comes at the cost of a damaged passivation (determined by PL measurements; cf. Fig. 3b) as Al completely penetrates the a-Si:H(i) layer. This would lead to low V_{ocS} (well below 700 mV) in final devices. Nevertheless, we find a trade-off where samples with both annealed contact and intact passivation (i.e. high PL intensity as shown in Fig. 3a) yield a ρ_c that is two to threefold lower than that of our Ag/ITO standard contact. In the following section, we report on IBC SHJ cells with such a carefully diffused Al/a-Si:H(p) contact.

B. IBC SHJ Solar Cells with Diffused Aluminium p-Contact

IBC SHJ solar cells featuring both Ag/ITO (standard contact) and Al (i.e. without TCO interlayer) for p-contact metallisation are fabricated. For all n-contacts, Ag/ITO is used. Except for the thickness of a-Si:H(p) and the metallisation scheme of that contact, all layers are identical in both cases. Final devices have to be annealed at moderate temperatures (below $190 \text{ }^\circ\text{C}$) over a prolonged period of time (90–120 min) in order to guarantee optimal contact formation by allowing for Al to diffuse into a-Si:H(p), ITO (where present) to crystallise, and sputter damage to be thermally cured (cf. section A for details). Note that TLM samples and final solar cells have been annealed on different hotplates, which entails using different set temperatures and annealing

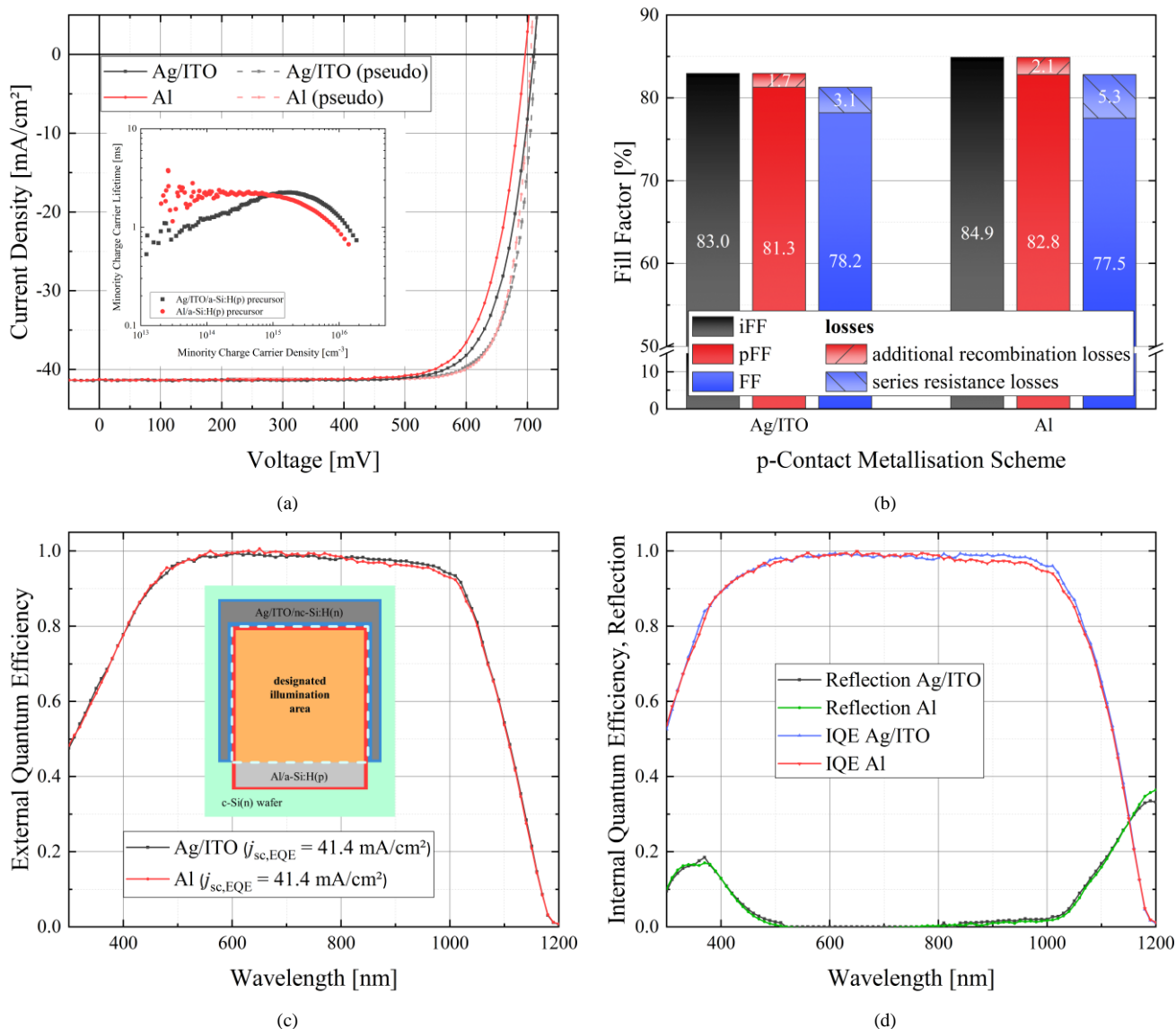


Fig. 4. (a) Illuminated one-sun (solid lines) and pseudo (dashed lines) current–voltage characteristics of the best IBC SHJ solar cells fabricated with different minority charge carrier contact metallisation schemes: a diffused Al (red) and an Ag/ITO contact (black); inset: measured minority charge carrier lifetime vs minority charge carrier density data that were used to calculate implied fill factors of both device types as described in the main text. (b) Fill factor losses of the two solar cells presented in (a). (c) external quantum efficiencies. (d) reflection and internal quantum efficiencies. Note that the QEs in the long wavelength regime are almost identical for both contact schemes despite optically less favourable properties of a direct Al contact. This is also evident from the EQE-integrated short-circuit current densities. A more detailed discussion can be found in the text. The inset in c shows a schematic (not to scale) of the structure (rear side) that has been used to measure the devices' EQE.

times. For TLM samples, a hotplate with a heat-reflecting lid and a larger thermal mass than that for solar cells has been used. For the same set temperature and annealing time, the first hotplate is therefore expected to impart a higher thermal energy budget and a more homogeneous heat transfer to the wafer than the second hotplate where a large part of the heat is also dissipated to surrounding ambient air.

In Fig. 4a, a direct comparison of the best solar cells' illuminated j - V characteristics (both Al and Ag/ITO) is depicted (solid lines); cell parameters are summarised in TABLE I. Implied fill factors (iFFs) are calculated from TrPCD measurements performed after patterning of the a-Si:H(i)/a-Si:H(p) stack and full-area deposition of the a-Si:H(i)/nc-Si:H(n) stack (repassivation) by using the method

described in [49] (black bars in Fig. 4b). The iFF can be interpreted as an upper FF limit, assuming ideal, only recombination limited solar cells and excluding the effect of parasitic resistances (i.e. infinite shunt resistance, R_{shunt} , and zero R_s). SunsVoc measurements of final devices are carried out in order to obtain pseudo j - V characteristics (dashed lines in Fig. 4a) and thereby the devices' pseudo fill factors (pFFs; red bars in Fig. 4b). Comparing these pseudo j - V characteristics with the illuminated j - V measured with a sun simulator, specifically the voltage difference at MPP, the devices' R_s can be calculated [50]. A difference between iFF and pFF is due to additional recombination losses upon contact formation (hatched red bars in Fig. 4b). For devices where this drop is very low, the chosen contact scheme and/or

TABLE I

SUMMARY OF RELEVANT DEVICE PARAMETERS OF THE BEST IBC SHJ SOLAR CELLS FABRICATED WITH DIFFERENT MINORITY CHARGE CARRIER CONTACT METALLISATION SCHEMES.

Metallisation Scheme	V_{oc} [mV]	j_{sc} [mA/cm ²]	FF [%]	PCE [%]	R_s [Ωcm ²]
Ag/ITO	710	41.3	78.2	22.9	0.6
Al	696	41.3	77.5	22.3	0.9

Abbreviations: silver/indium tin oxide (Ag/ITO), aluminium (Al), open-circuit voltage (V_{oc}), short-circuit current density (j_{sc}), fill factor (FF), power conversion efficiency (PCE), and series resistance (R_s). The latter is determined by the SunsVoc method as explained in [48].

fabrication process does not significantly impair the passivation quality. A passivation that is degraded upon contact formation leads to increased recombination at the semiconductor/metal interface and thereby a strongly decreased V_{oc} . In general, poor surface passivation is due to an increased interface defect density that can also impair charge carrier extraction [47]. If such degradation is caused by contact formation, this is revealed by a huge difference between iFF and pFF. For the Al contacted solar cells investigated here, a slightly lower V_{oc} of 700 ± 4 mV (as compared to 710 ± 5 mV of the standard contact) is found, probably due to increased recombination at the diffused Al/a-Si:H(p) contact (Fig. 4b). From Fig. 4b, it can further be seen that Al contacted devices feature an approximately 1.9%_{abs} higher iFF than their Ag/ITO counterpart. At this point, only amorphous silicon has been deposited and partly patterned (cf. above), but Al devices feature thicker p-doped layers (twice the thickness as compared to Ag/ITO devices) in order to provide ‘room’ for Al diffusion into a-Si:H(p) as has been pointed out in the Experimental section. Note that the iFF of Ag/ITO devices could potentially be improved by using thicker doped layers as well. Despite similar minority charge carrier lifetimes of about 2.1 ms at an excess charge carrier density of 10^{15} cm⁻³ in both cases (cf. inset of Fig. 4a), Al devices feature a much better low-intensity response (i.e. below $\Delta n = 10^{15}$ cm⁻³), probably due to the thicker p-doped layers providing better field-effect passivation and thereby a higher iFF. While calculating the iFFs of different device types, it was also found that wafers used for Al/a-Si:H(p) precursors had a slightly lower wafer resistivity (and thereby higher doping concentration) than those used for Ag/ITO/a-Si:H(p) precursors (1.3 Ωcm vs 2.6 Ωcm). We note that this is not an intentional design choice since wafers with identical properties as per manufacturer specifications were chosen for both device categories. The difference between pFF and FF is usually due to series resistance-related losses (hatched blue bars in Fig. 4b). It is larger than that between iFF and pFF, and thus the R_s contribution dominates the FF losses. For Al devices, there is a 5 mV drop between pseudo- V_{oc} and final V_{oc} (both are identical in Ag/ITO devices) that probably stem from using different setups with different calibrations and the substrate temperature not being controlled in our SunsVoc setup. It is surprising that, despite a lower $\rho_{c,p}$, Al devices feature increased series-resistance losses. In the absence of experimental evidence pointing to other mechanisms, the final drop from pFF to FF is most likely

explained by series-resistance losses. This circumstance is puzzling and requires further investigation since it is as of yet unclear why the p-contact’s lower contact resistivity does not translate into an increased FF. If this were the case and the full potential of the observed decrease in ρ_c of an Al/a-Si:H(p) contact (150–200 mΩcm² lower as compared to an Ag/ITO/a-Si:H(p) contact; cf. section A) could be exploited, one would expect an FF gain of 0.8–1.4%. This issue needs to be tackled in the future. The FF of the best Al contacted device (77.5%) is however still comparable to the best Ag/ITO solar cell (78.2%), yielding PCEs of 22.3% and 22.9% respectively.

Although the near-IR reflectivity of an Al film is lower than that of an Ag/ITO stack [51], interestingly, no loss in short-circuit current density (j_{sc}) occurs, which is also confirmed by external (Fig. 4c) and internal quantum efficiency measurements (Fig. 4d). For Al devices, a slightly lower EQE and IQE is visible in the long-wavelength regime (> 800 nm), which is counteracted by higher response in the visible part of spectrum. Ideally there should be no difference in the visible range because the front-side layer stack is nominally identical for both devices and the discrepancy probably stems from unintentional minor variations during device fabrication. Manually shifting the Al device’s EQE curve in the short wavelength region so that it aligns with that of the Ag/ITO device, results in an integrated j_{sc} of 41.2 mA/cm², which still represents a rather marginal current loss. In SHJ solar cells, a rear-side TCO is usually introduced to suppress parasitic plasmonic absorption that would occur at a direct metal/Si interface [52]. On the other hand, inserting said TCO can lead to free-carrier absorption of long-wavelength photons in the red and near-infrared part of the spectrum [53]. Both effects impact the j_{sc} and their respective contribution to current losses need to be carefully considered. In case of the devices investigated here, parasitic plasmonic absorption in the metal contact and free-carrier absorption in the ITO appear to be of similar magnitude so that the current losses are similar in both cases. This will be investigated by means of optical simulations in the next section.

C. Optical Device Simulation

In this section, the MATLAB-based simulation programme GenPro4 [54] is used to assess the optical properties of the investigated p-contact stacks. For the simulation, a 280 μm thick c-Si absorber with pyramidal texture at its front and flat surface at its rear side is sandwiched between two infinitely thick layers of air. The wafer is treated as an incoherent medium, while all other materials are added as coherent layers to either side of the absorber. Complex refractive indices (n, κ) are either measured in-house by means of spectroscopic ellipsometry or taken from literature (cf. TABLE II for details). It is challenging to implement an Al-interdiffused a-Si:H(p) layer into the simulations. Simply stacking both materials is certainly physically incorrect. However, taking literature data for generic aluminium silicide is not helpful either because those are generally reported for eutectic alloys

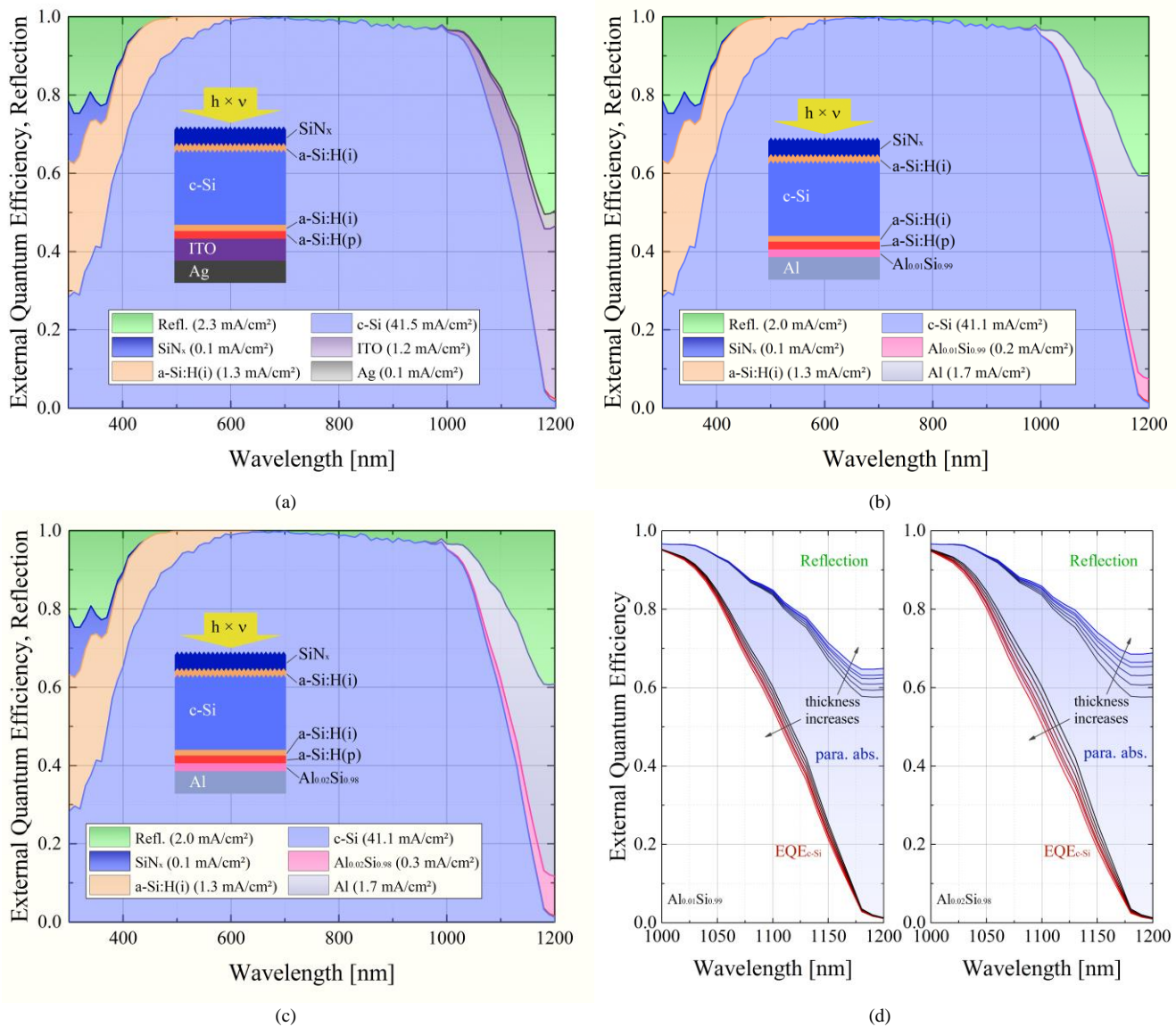


Fig. 5. Simulated external quantum efficiencies (EQEs) of devices with different rear contacts: (a) Ag/ITO, (b) nanocrystalline p-type silicon doped with 1% Al and Al metallisation, (c) same as in (b) but with 2% Al doping. The insets in a–c show schematics (not to scale) of the investigated layer stacks. (d) Simulated influence of Al_xSi_y layer thickness on the c-Si absorber's near-IR EQE (EQE_{c-si}) for Al doping concentrations of 1 and 2% (left and right respectively); the area highlighted in blue marks the combined parasitic absorption (para. abs.) in the rear-side layer stack (i.e. Al + Al_xSi_y).

that are Al-rich (volume fraction above 85%) and form only at temperatures of several hundred degrees Celsius [22],[55], which is not the case here. It is more likely that the resulting interlayer consists of a partially crystallised silicon layer doped with an Al concentration of not more than 1–2% [22]. The Al_xSi_y layer used here is therefore calculated from n, κ data of nc-Si:H (measured in-house) and Al (for concentrations of 1 and 2%; taken from [56]) by using an effective medium approach [57]. GenPro4's ray tracing algorithm is used to compute the photon flux absorbed in each layer within a wavelength range of 300–1200 nm. Here, current generated in the c-Si absorber represents the device's j_{sc} whereas current losses in other layers are attributed to either reflection (air) or parasitic absorption (all other layers). Note that in GenPro4 only devices consisting of stacked layers with full-area coverage can be modelled, an IBC solar cell,

however, features a more complex geometry due to its laterally patterned contacts. Therefore only the p-contact is simulated, which leads to a structure similar to what is actually used to determine the EQE of our devices (cf. inset of Fig. 4c). Simulation results for each considered device architecture (Ag/ITO/a-Si:H(p), Al/Al_{0.01}nc-Si:H(p)_{0.99}/a-Si:H(p), and Al/Al_{0.02}nc-Si:H(p)_{0.98}/a-Si:H(p)) are shown in Fig. 5a–c along with schematics of the used layer stacks. It becomes apparent that although only small amounts of Al are introduced in a relatively thin a-Si:H layer at the rear side, the resulting aluminium silicide contributes appreciably to current losses occurring in the near-IR (j_{sc} loss up to 0.3 mA/cm² for the 2% variety). This effect is illustrated further in Fig. 5d for various Al_xSi_y layer thicknesses from 0–23 nm, highlighting the wavelength region from 1000–1200 nm. The overall photon flux absorbed in the c-Si absorber, Al_xSi_y, and Al stays

TABLE II
MATERIALS USED IN OPTICAL DEVICE SIMULATION. ‘SOURCE’ REFERS TO THE ORIGIN OF COMPLEX REFRACTIVE INDEX DATA.

Material	Thickness [nm]	Source
air	infinite	constant: $n = 1, \kappa = 0$
SiN _x	70	[57]
a-Si:H(i) (front side)	7.5	in-house
c-Si(n)	280×10^3	[58]
a-Si:H(i) (rear side)	5	in-house
a-Si:H(p)	9 or 13 ^a	in-house
ITO	150	in-house
Ag	1.5×10^3	[56]
Al _x Si _y	5 ^b	in-house and [56] ^c
Al	2.0×10^3	[56]

^aAs described in section II, the a-Si:H(p) layer thickness is different for Ag/ITO (9 nm) and Al devices (13 nm)

^bThickness of the modified a-Si:H(p) portion underneath Al as described in the text; the combined thickness of Al_xSi_y and a-Si:H(p) is 18 nm, thus twice as thick as in Ag/ITO devices

^cCalculated from n, κ data of nc-Si:H (measured in-house) and Al (taken from [56]) for Al concentrations of 1 and 2% using the effective medium approach; see the text for further details

roughly constant, equivalent to a combined photocurrent of 43.1 mA/cm² for all investigated thicknesses. This indicates that the absorption is only redistributed between these components and that current loss occurring in the IR is chiefly due to additional parasitic absorption in the rear-side contact stack. A total of 1.2 mA/cm² are lost due to parasitic absorption if the entire former a-Si:H(i,p) stack is crystallised (23 nm thick layer of 2% Al_xSi_y). Trends for both Al concentrations are similar, with the 2% case leading to more severe current losses. Even for the best investigated case (i.e. 5 nm Al_{0.01}nc Si:H(p)_{0.99}), Al devices lag behind their Ag/ITO counterparts by approximately 0.3 mA/cm², which contradicts the observations made before. A possible explanation is that in the simulation a homogeneous layer of a rather absorptive Al_xSi_y layer is assumed. In an earlier publication, however, we have estimated that the Al affected area in these devices cannot be larger than 20% [27]. Moreover, only the p-contact of our IBC cells features aluminium metallisation (with the n-contact being Ag/ITO), which further alleviates any negative optical effect this contact might have. Lastly, while an AM1.5g spectrum is only (however closely) approximated in our measurements, it is exactly represented in the simulation, which might lead to minor spectral differences between simulation and experiment.

D. Simulation of Diffused Aluminium Contact Formation

In order to better understand the observed electrical behaviour of devices featuring a diffused Al/a-Si:H(p) contact, electrical equivalent circuit simulations are conducted. IBC SHJ solar cells can be well described with a two-diode model [6]. Additionally, as proposed in literature [43],[59] and discussed in section A, the as-deposited Al/a-Si:H(p) contact exhibits rectifying behaviour whereas after annealing it is ohmic. This transition during contact formation can be sufficiently described by an extended equivalent circuit model featuring an antiparallel Schottky diode in parallel to a shunt resistance ($R_{sh,Schottky}$) as depicted in Fig. 6a. This model was introduced in [60] and has been used later to describe the

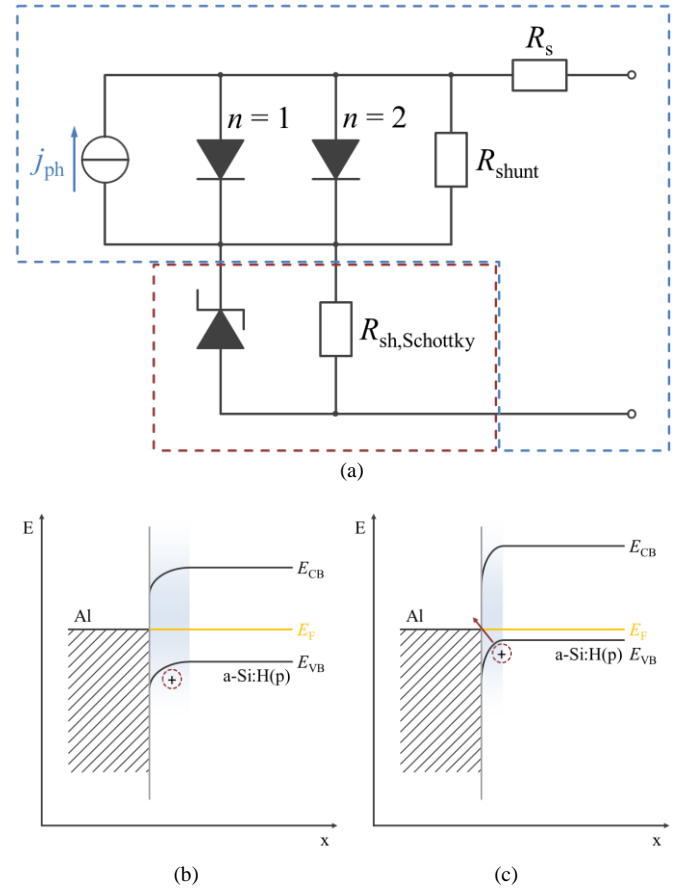


Fig. 6. (a) Electrical equivalent circuit used for device modelling, after [59]. A standard two-diode model (dashed blue outline) is extended at the p-contact by an antiparallel Schottky diode and a shunt resistor ($R_{sh,Schottky}$) (dashed red outline). If $R_{sh,Schottky}$ is sufficiently small, the Schottky diode is effectively shunted and the solar cell behaves as in a regular two-diode configuration. Otherwise, the Schottky diode impedes proper current extraction from the device. (b) Schematic equilibrium band line-up of an Aluminium/p-type hydrogenated amorphous silicon contact for low, and (c) high doping concentration in a-Si:H(p) at the interface with Al. The case depicted in (c) leads to efficient hole tunnelling (red arrow). E_F , E_{CB} , and E_{VB} denote the energies of the Fermi level, conduction band edge, and valence band edge. Space charge regions are marked blue in order to illustrate different doping concentrations.

electrical behaviour of different high-efficiency solar cell architectures, such as PERC (passivated emitter and rear cell), PERL (passivated emitter, rear locally diffused), and SHJ [19],[59],[61]. It has also been used to describe so-called s-shaped j - V characteristics in SHJ solar cells [62]. The magnitude of $R_{sh,Schottky}$ determines whether the rectifying Schottky circuit (dashed red outline in Fig. 6a) or an ohmic contact represented by the basic two-diode equivalent circuit (dashed blue outline in Fig. 6a) predominates for a given external voltage. For high $R_{sh,Schottky}$, the overall solar cell behaviour is governed by the antiparallel Schottky diode and current extraction is impeded for higher voltages [62], depending on the Schottky diode's saturation current density (j_s) [60]. For low $R_{sh,Schottky}$, the Schottky diode is effectively shunted and therefore no longer influences current extraction. For the purpose of this work, the diode characteristics of the two ‘regular diodes’ (dashed blue outline in Fig. 6a) are extracted by fitting the two-diode model without the Schottky

diode and $R_{sh,Schottky}$ to dark j - V characteristics of a well-performing annealed Al contacted solar cell. The ideality factors (n_1 and n_2) are set to 1 and 2 respectively, R_s is determined by the SunsVoc method as described in section B, and R_{shunt} is known from illuminated j - V measurements. The ideality factor of the Schottky diode is set to 1.04 according to [43] and its j_s can be calculated by using (1) [29].

$$j_s = A^* \cdot T^2 \cdot \exp\left(\frac{-q \cdot \varphi_B}{k \cdot T}\right) \quad (1)$$

Here, A^* denotes the Richardson constant ($32 \text{ Acm}^{-2}\text{K}^{-2}$ for p-type silicon [29]), T the absolute temperature, q the elementary charge, k the Boltzmann constant, and φ_B the Schottky barrier height. In the simplest scenario, the barrier height for holes is given by the Schottky-Mott rule as the difference between the metal's work function (Φ_m) and the electron affinity of the semiconductor subtracted from its band gap (in other words: between Φ_m and the semiconductors ionisation energy) [63]. However, this approach is not applicable here because metal/silicon interface states can pin the Fermi level (E_F) close to midgap position regardless of the contact material's work function [64]. The Schottky barrier height for a diffused Al/crystalline p-type silicon contact has been reported to 0.4–0.6 eV [59] whereas the Schottky-Mott rule yields 0.89 eV. Here, φ_B between Al and *amorphous* p-type silicon is the relevant parameter, and we obtain an estimate for φ_B at this interface by applying the transitivity rule for heterojunctions: as the p-contact is being investigated, we add the valence-band offset, ΔE_{VB} , between crystalline and amorphous silicon to the known Al/c-Si(p) barrier height. Depending on the hydrogen content (C_H), ΔE_{VB} has been reported to be in the range of 200–450 meV (for C_H ranging from 10–25%) [65], resulting in a φ_B of the diffused Al/a-Si:H(p) contact of $\Delta E_{VB} + \varphi_B \sim 0.6$ –1.05 eV. The upper boundary represents a rather large energetic barrier, which further explains the very high ρ_c s found for as-deposited Al/a-Si:H(p) contacts in section A. However, as the contact is annealed and Al diffusion occurs, the doping concentration (N_A) in a-Si:H(p) rises at the interface, which enables tunnelling [62] (Fig. 6b and c). In the tunnelling case, ρ_c strongly depends on N_A . A sufficiently high doping concentration ($> 10^{19} \text{ cm}^{-3}$) results in an ohmic contact as ρ_c becomes increasingly independent of the barrier height [63]. Using (2), one can then calculate the tunnel-dominated ρ_c [63].

$$\rho_c = \frac{k}{q \cdot T \cdot A^*} \cdot \exp\left(\frac{4 \cdot \pi \cdot \sqrt{\varepsilon_0 \cdot \varepsilon_r \cdot m_p \cdot e_{\text{eff}}}}{h} \cdot \frac{\varphi_B}{\sqrt{N_A}}\right) \quad (2)$$

Here, h denotes Planck's constant, ε_0 the permittivity in

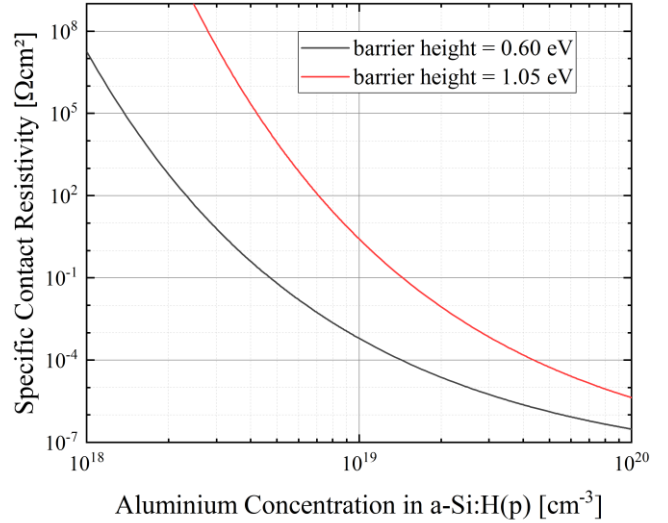


Fig. 7. Specific contact resistivity of a diffused Al/a-Si:H(p) contact at high doping concentrations, enabling thus tunnelling of minority charge carriers. Calculations are conducted for two different Schottky barrier heights as discussed in the text.

vacuum, ε_r the dielectric constant, and $m_{p,eff}$ the effective tunnelling mass of holes, reported to $0.1 \times m_0$ for SHJ devices based on a-Si:H contacts [66],[67] where m_0 is the electron rest mass. ε_r values of 11.9 [63] and 10.0 [68] have been reported for crystalline silicon and a-Si:H respectively. In Fig. 7, the resulting ρ_c s for N_A s ranging from 10^{18} – 10^{20} cm^{-3} and φ_B s of 0.6 eV (black line) and 1.05 eV (red line) are depicted. Values of $< 1 \text{ } \Omega\text{cm}^2$ are achieved for $N_A > 3.6 \times 10^{18} \text{ cm}^{-3}$ (0.6 eV) or $> 1.1 \times 10^{19} \text{ cm}^{-3}$ (1.05 eV). Obtaining $500 \text{ m}\Omega\text{cm}^2$, which is competitive to an Ag/ITO/a-Si:H(p) contact, necessitates an N_A of $> 5.2 \times 10^{18} \text{ cm}^{-3}$ (0.6 eV) or $> 1.6 \times 10^{19} \text{ cm}^{-3}$ (1.05 eV). To put these values into perspective: Al concentrations of fully crystallised silicon films formed by aluminium-induced crystallisation of amorphous silicon on glass have been reported to be as high as $3 \times 10^{19} \text{ cm}^{-3}$ [69]. It should be noted though that these devices have been exposed to temperatures in the range of 375–525 °C. HAQUE *et al.* have reported on the interaction mechanism between Al and a-Si:H at low temperatures (between 150–200 °C) and describe the formation of a ‘heavily doped’ (not specified) thin layer between Al and amorphous silicon consisting of Al-rich p-type crystallites. However, since here the doping concentration after annealing has not been measured, it is as of yet unclear whether such high Al concentrations are obtained for low annealing temperatures. It is therefore likely that a combination of Al doping and crystallisation of (former) amorphous silicon leads to the observed decrease in contact resistivity, especially

TABLE III
LTSPICE PARAMETERS USED FOR MODELLING THE CONTACT FORMATION OF IBC SHJ SOLAR CELLS WITH DIFFUSED ALUMINIUM MINORITY CHARGE CARRIER CONTACT IN LTSPICE, CF. FIG. 8A.

j_{photo} [mA/cm²]	$j_{0,1}$ [A/cm²]	$j_{0,2}$ [A/cm²]	j_s [A/cm²]	n_1	n_2	n_{Schottky}	R_s [Ωcm²]	R_{shunt} [Ωcm²]	$R_{\text{sh,Schottky}}$ [Ωcm²]
40.3	4.5×10^{-14}	1.4×10^{-9}	5.9×10^{-15}	1	2	1.04	1.6	1200	0–1000

Abbreviations: photogenerated current density (j_{photo}), saturation current density and ideality factor of diode 1, diode 2, and the Schottky diode ($j_{0,1}$, $j_{0,2}$, j_s , n_1 , n_2 , and n_{Schottky}), series resistance (R_s), shunt resistance (R_{shunt}), and shunt resistance of the Schottky diode ($R_{\text{sh,Schottky}}$).

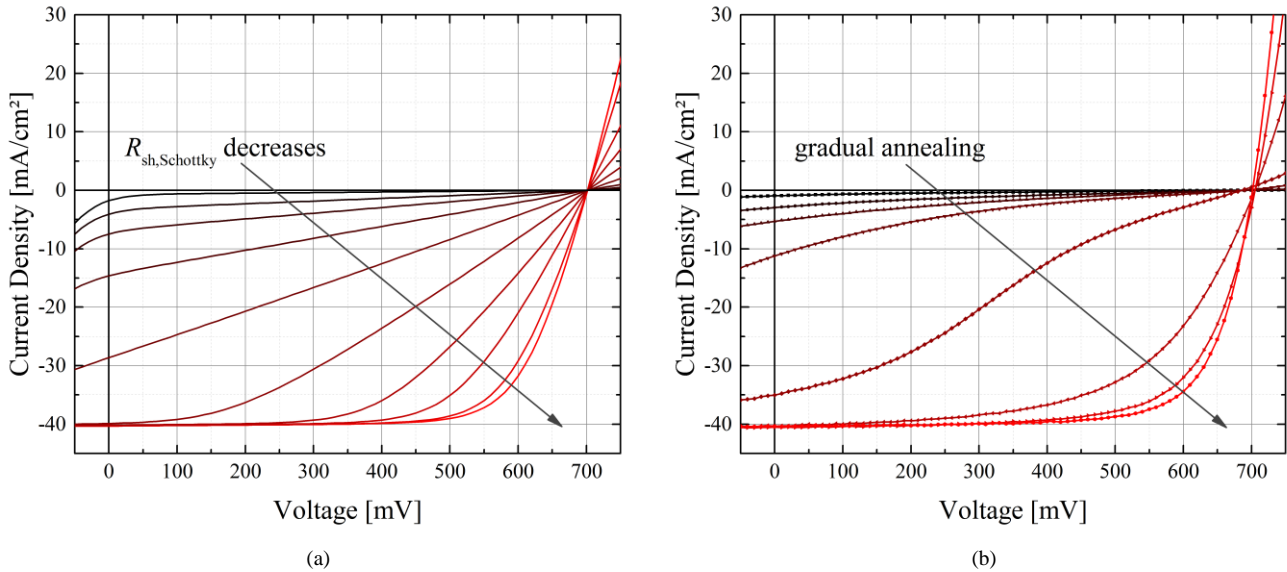


Fig. 8. (a) Modelled and (b) measured illuminated current–voltage characteristics of IBC SHJ solar cells featuring diffused Aluminium metallisation for the minority charge carrier contact during different stages of contact formation upon annealing. Measurements are carried out under STC, modelling is conducted in LTspice by simulating the equivalent circuit depicted in Fig. 5a with the parametrisation given in TABLE III.

since the default surface doping concentration in the used a-Si:H(p) layer is already in the order of 10^{19} cm^{-3} .

Electrical equivalent circuit simulations have been conducted in LTspice by using the model introduced above (Fig. 6a); modelling parameters are given in TABLE III. All parameters are kept constant except for $R_{sh,Schottky}$, which is swept from 0–1 $\text{k}\Omega\text{cm}^2$ to represent different states of Al/a-Si:H(p) interdiffusion and contact formation: as-deposited rectifying mode (1 $\text{k}\Omega\text{cm}^2$), effective shunting of the Schottky diode (0 Ωcm^2), and various stages of contact formation (values in between). In Fig. 8a, the resulting modelled j – V characteristics are depicted, which are in good agreement with measured results (Fig. 8b; obtained by successive annealing and measuring steps). The V_{oc} s of the experimental devices gradually shift to lower values as the samples are further annealed. Electrically, this could be modelled with a gradual increase in dark saturation current density j_0 especially of the $n=1$ diode. For instance, increasing j_0 from $4.5 \times 10^{-14} \text{ A/cm}^2$ to $5.5 \times 10^{-14} \text{ A/cm}^2$ results in a V_{oc} decrease of $\sim 4 \text{ mV}$. This circumstance is, however, not regarded in the simulation and thus the V_{oc} remains constant in all cases.

IV. CONCLUSION

Silicon heterojunction (SHJ) solar cells with interdigitated back-contacts (IBC) featuring different contact stacks are investigated. The transfer-length method is used to extract the specific contact resistivity, ρ_c , of a standard silver/indium tin oxide and a direct aluminium contact (omitting ITO) for both the p and n-contact. The p-contact is known to contribute by far the biggest share to the overall series resistance (R_s) in IBC SHJ solar cells [8],[12],[13]. It is found that applying a carefully annealed and thereby diffused and crystallised Al/a-Si:H(p) contact is an effective mean to cut the ρ_c in half as compared to Ag/ITO/a-Si:H(p). IBC SHJ cells with Al p

and ITO/Ag n-contact yield a fill factor (FF) of 77.5% and a power conversion efficiency (PCE) of 22.3%, which is only marginally worse than the best reference device with Ag/ITO for both contacts (FF 78.2%, PCE 22.9%). The biggest difference between the two concepts is a 14 mV lower open-circuit voltage (V_{oc}) and higher R_s of the Al contacted solar cells (696 mV vs 710 mV and 0.9 Ωcm^2 vs 0.6 Ωcm^2). This hints at two potential risks when using an Al contact in SHJ solar cells. The first aspect (a lower V_{oc}) is probably caused by Al spiking through the passivation layer and thereby causing locally increased recombination losses at the diffused and crystallised Al/a-Si:H(p) contact. The second matter is a higher R_s at device level, which is not yet fully understood and requires further investigation. However, there should be no fundamental problem with applying Al as a hole contact since the results of TLM measurements suggest reduced contact resistivity and Al spiking can be avoided (and thereby the surface passivation kept intact) by controlling annealing conditions. Remarkably, no loss in short-circuit current density (j_{sc}) occurs despite the lower reflectivity of the direct Al/Si contact. As-deposited Al forms a rectifying (or at least highly resistive) contact with a-Si:H(p) as indicated by a high ρ_c and barely any current extraction for positive bias voltages. As has been demonstrated previously, Al starts to diffuse into a-Si:H(p) and forms partially crystallised aluminium silicide upon annealing at moderate temperatures ($160 \text{ }^\circ\text{C} < T < 190 \text{ }^\circ\text{C}$) [21]. This leads to a drastic decrease in ρ_c as the aluminium silicide partially crystallises and the Al doping concentration (N_A) in a-Si:H(p) increases at the interface, which eventually enables efficient tunnelling of holes and results in the formation of an ohmic contact. A classic two-diode electrical equivalent circuit model extended by an antiparallel Schottky diode and a shunt resistor is found to sufficiently describe the electrical behaviour of the investigated devices during contact formation.

ACKNOWLEDGMENT

The authors would like to thank Anna Belen Morales Vilches and Alvaro Tejada Esteves for spectroscopic ellipsometry measurements. The determined complex refractive index data were used in the optical simulation section. Kerstin Jacob and Mona Wittig are thanked for texturing and RCA cleaning of the used wafers. Furthermore, the HZB institute PVcomB is recognised for providing deposition and measurement equipment.

REFERENCES

- [1] M. Taguchi, A. Yano, S. Tohoda, K. Matsuyama, Y. Nakamura, T. Nishiwaki, K. Fujita, and E. Maruyama, "24.7% record efficiency HIT solar cell on thin silicon wafer," *IEEE J PHOTOVOLT*, vol. 4, pp. 96–99, 2013.
- [2] S. De Wolf, C. Ballif and M. Kondo, "Kinetics of a-Si: H bulk defect and a-Si: H/c-Si interface-state reduction," *Phys. Rev. B*, vol. 85, p. 113302, 2012.
- [3] K. Yoshikawa, H. Kawasaki, W. Yoshida, T. Irie, K. Konishi, K. Nakano, T. Uto, D. Adachi, M. Kanematsu, H. Uzu, and K. Yamamoto, "Silicon heterojunction solar cell with interdigitated back contacts for a photoconversion efficiency over 26%," *Nat. Energy*, vol. 2, p. 17032, 2017.
- [4] M. A. Green, E. D. Dunlop, D. H. Levi, J. Hohl-Ebinger, M. Yoshita, and A. W. Y. Ho-Baillie, "Solar cell efficiency tables (version 54)," *Prog Photovolt Res Appl.*, vol. 27, pp. 565–575, 2019.
- [5] M. Tucci, L. Serenelli, E. Salza, S. De Iulius, L. J. Geerligs, G. De Cesare, D. Caputo, and M. Ceccarelli, "Novel scheme of amorphous/crystalline silicon heterojunction solar cell," in *Proc. 22nd Eur. Photovoltaic Sol. Energy Conf*, Milan, Italy, 2007, pp. 1600–1603.
- [6] A. Tomasi, B. Paviet-Salomon, D. Lachenal, S. M. Nicolas, A. Descoedres, J. Geissbühler, S. De Wolf, and C. Ballif, "Back-contacted silicon heterojunction solar cells with efficiency > 21%," *IEEE J PHOTOVOLT*, vol. 4, pp. 1046–1054, 2014.
- [7] A. Tomasi, B. Paviet-Salomon, Q. Jeangros, J. Haschke, G. Christmann, L. Barraud, A. Descoedres, J. P. Seif, S. Nicolay, M. Despeisse, S. De Wolf, and C. Ballif, "Simple processing of back-contacted silicon heterojunction solar cells using selective-area crystalline growth," *Nat. Energy*, vol. 2, p. 17062, 2017.
- [8] B. Paviet-Salomon, A. Tomasi, D. Lachenal, N. Badel, G. Christmann, L. Barraud, A. Descoedres, J. Geissbühler, A. Faes, Q. Jeangros, J. P. Seif, S. Nicolay, B. Strahm, S. De Wolf, C. Ballif, and M. Despeisse, "Interdigitated back contact silicon heterojunction solar cells featuring an interband tunnel junction enabling simplified processing," *Sol. Energy*, vol. 175, pp. 60–67, 2018.
- [9] P. Wagner, J.-C. Stang, M. Mews, A. B. Morales-Vilches, B. Stannowski, B. Stegemann, and L. Korte, "Interdigitated back contact silicon heterojunction solar cells: Towards an industrially applicable structuring method," in *AIP Conf. Proc.*, Lausanne, Switzerland, 2018, p. 060001.
- [10] M. Xu, T. Bearda, M. Filipič, H. S. Radhakrishnan, I. Gordon, J. Szlufcik, and J. Poortmans, "Simple emitter patterning of silicon heterojunction interdigitated back-contact solar cells using damage-free laser ablation," *Sol. Energy Mater. Sol. Cells*, vol. 186, pp. 78–83, 2018.
- [11] H. Sivaramakrishnan Radhakrishnan, M. D. G. Uddin, M. Xu, J. Cho, M. Ghannam, I. Gordon, J. Szlufcik, and J. Poortmans, "A novel silicon heterojunction IBC process flow using partial etching of doped a-Si: H to switch from hole contact to electron contact in situ with efficiencies close to 23%," *Prog Photovolt Res Appl.*, vol. 27, no. 11, pp. 959–970, 2019.
- [12] D. Lachenal, P. Papet, B. Legradic, R. Kramer, T. Kössler, L. Andreetta, N. Holm, W. Frammelsberger, D. L. Baetzner, B. Strahm, L. L. Senaud, J. W. Schüttauf, A. Descoedres, G. Christmann, S. Nicolay, M. Despeisse, B. Paviet-Salomon, and C. Ballif, "Optimization of tunnel-junction IBC solar cells based on a series resistance model," *Sol. Energy Mater. Sol. Cells*, vol. 200, p. 110036, 2019.
- [13] M. Leilaoui, W. Weigand, M. Boccard, J. Y. Zhengshan, K. Fisher, and Z. C. Holman, "Contact resistivity of the p-type amorphous silicon hole contact in silicon heterojunction solar cells," *IEEE J PHOTOVOLT*, vol. 10, no. 1, pp. 54–62, 2019.
- [14] M. Bivour, S. Schröer, and M. Hermle, "Numerical analysis of electrical TCO/a-Si: H (p) contact properties for silicon heterojunction solar cells," *Energy Procedia*, vol. 38, pp. 658–669, 2013.
- [15] G. Hautier, A. Miglio, G. Ceder, G.-M. Rignanese, and X. Gonze, "Identification and design principles of low hole effective mass p-type transparent conducting oxides," *Nat. Commun.*, vol. 4, p. 2292, 2013.
- [16] A. N. Fioretti and M. Morales-Masis, "Bridging the p-type transparent conductive materials gap: synthesis approaches for disperse valence band materials," *J. Photonics Energy*, vol. 10, p. 042002, 2020.
- [17] M. Morales-Masis, S. De Wolf, R. Woods-Robinson, J. W. Ager, and C. Ballif, "Transparent electrodes for efficient optoelectronics," *Adv. Electron. Mater.*, vol. 3, no. 5, p. 1600529, 2017.
- [18] A. Kanevce and W. K. Metzger, "The role of amorphous silicon and tunneling in heterojunction with intrinsic thin layer (HIT) solar cells," *J. Appl. Phys.*, vol. 105, p. 094507, 2009.
- [19] R. V. K. Chavali, J. R. Wilcox, B. Ray, J. L. Gray, and M. A. Alam, "Correlated nonideal effects of dark and light I–V characteristics in a-Si/c-Si heterojunction solar cells," *IEEE J PHOTOVOLT*, vol. 4, pp. 763–771, 2014.
- [20] A. Louwen, W. Van Sark, R. Schropp, and A. Faaij, "A cost roadmap for silicon heterojunction solar cells," *Sol. Energy Mater. Sol. Cells*, vol. 147, pp. 295–314, 2016.
- [21] M. S. Haque, H. A. Naseem, and W. D. Brown, "Interaction of aluminum with hydrogenated amorphous-silicon at low-temperatures," *J. Appl. Phys.*, vol. 75, pp. 3928–3935, 1994.
- [22] M. S. Haque, H. A. Naseem, and W. D. Brown, "Aluminum-induced crystallization and counter-doping of phosphorous-doped hydrogenated amorphous silicon at low temperatures," *J. Appl. Phys.*, vol. 79, pp. 7529–7536, 1996.
- [23] D. K. Schroder and D. L. Meier, "Solar cell contact resistance—A review," *IEEE Trans. Electron Devices*, vol. 31, pp. 637–647, 1984.
- [24] M. Bivour, C. Reichel, M. Hermle, and S. W. Glunz, "Improving the a-Si: H(p) rear emitter contact of n-type silicon solar cells," *Sol. Energy Mater. Sol. Cells*, vol. 106, pp. 11–16, 2012.
- [25] S. Ishihara, T. Hirao, K. Mori, M. Kitagawa, M. Ohno, and S. Kohiki, "Interaction between n-type amorphous hydrogenated silicon films and metal electrodes," *J. Appl. Phys.*, vol. 53, pp. 3909–3911, 1982.
- [26] J. Bullock, D. Yan, Y. Wan, A. Cuevas, B. Demareux, A. Hessler-Wyser, and S. De Wolf, "Amorphous silicon passivated contacts for diffused junction silicon solar cells," *J. Appl. Phys.*, vol. 115, p. 163703, 2014.
- [27] J.-C. Stang, J. Haschke, M. Mews, A. Merkle, R. Peibst, B. Rech, and L. Korte, "Aluminium metallisation for interdigitated back-contact silicon heterojunction solar cells," *Jpn. J. Appl. Phys.*, vol. 56, p. 08MB22, 2017.
- [28] A. B. Morales-Vilches, E. Wang, T. Henschel, M. Kubicki, A. Cruz, S. Janke, L. Korte, R. Schlatmann, and B. Stannowski, "Improved Surface Passivation by Wet Texturing, Ozone-Based Cleaning, and Plasma-Enhanced Chemical Vapor Deposition Processes for High-Efficiency

- Silicon Heterojunction Solar Cells,” *Phys. Status Solidi A*, vol. 217, p. 1900518, 2020.
- [29] D. K. Schroder, “Contact resistance, Schottky barriers, and electromigration,” in *Semiconductor Material and Device Characterization*, 2nd ed. New York, NY, USA: Wiley, 1998, pp. 156–169.
- [30] R. A. Sinton and A. Cuevas, “Contactless determination of current–voltage characteristics and minority-carrier lifetimes in semiconductors from quasi-steady-state photoconductance data,” *Appl. Phys. Lett.*, vol. 69, pp. 2510–2512, 1996.
- [31] R. A. Sinton and A. Cuevas, “A quasi-steady-state open-circuit voltage method for solar cell characterization,” in *Proceedings of the 16th European Photovoltaic Solar Energy Conference*, Glasgow, UK, 2000, pp. 1–4.
- [32] Analog Devices, “LTspice”, <https://www.analog.com/en/design-center/design-tools-and-calculators/ltspice-simulator.html>, time stamp: 14.02.2020.
- [33] E. Wang, A. B. Morales-Vilches, S. Neubert, A. Cruz, R. Schlatmann, and B. Stannowski, “A simple method with analytical model to extract heterojunction solar cell series resistance components and to extract the a-Si:H(i/p) to transparent conductive oxide contact resistivity,” in *AIP Conf. Proc.*, Leuven, Belgium, 2019, p. 040022.
- [34] L. Basset, W. Favre, D. Muñoz, and J. P. Vilcot, “Series resistance breakdown of silicon heterojunction solar cells produced on CEA-INES pilot line,” in *Proc. 35th Eur. Photovoltaic Sol. Energy Conf*, Brussels, Belgium, 2018, pp. 721–724.
- [35] H. Schade and Z. E. Smith, “Contact resistance measurements for hydrogenated amorphous silicon solar cell structures,” *J. Appl. Phys.*, vol. 59, pp. 1682–1687, 1986.
- [36] K. U. Ritzau, T. Behrendt, D. Palaferri, M. Bivour, and M. Hermle, “Hydrogen doping of Indium Tin Oxide due to thermal treatment of hetero-junction solar cells,” *Thin Solid Films*, vol. 599, pp. 161–165, 2016.
- [37] S. Y. Herasimenka, W. J. Dauksher, M. Boccard, and S. Bowden, “ITO/SiOx:H stacks for silicon heterojunction solar cells,” *Sol. Energy Mater. Sol. Cells*, vol. 158, pp. 98–101, 2016.
- [38] A. Cruz, F. Ruske, A. Eljarrat, P. P. Michalowski, A. B. Morales-Vilches, S. Neubert, E. Wang, C. T. Koch, B. Szyszka, R. Schlatmann, and B. Stannowski, “Influence of Silicon Layers on the Growth of ITO and AZO in Silicon Heterojunction Solar Cells,” *IEEE J PHOTOVOLT*, vol. 10, no. 2, pp. 703–709, 2019.
- [39] B. Demareux, S. De Wolf, A. Descoedres, Z. Charles Holman, and C. Ballif, “Damage at hydrogenated amorphous/crystalline silicon interfaces by indium tin oxide overlayer sputtering,” *Appl. Phys. Lett.*, vol. 101, p. 171604, 2012.
- [40] S. De Wolf, H. Fujiwara, and M. Kondo, “Impact of annealing on passivation of a-Si: H/c-Si heterostructures,” in *2008 33rd IEEE Photovoltaic Specialists Conference*, San Diego, CA, USA, 2008, pp. 1–4.
- [41] C. Messmer, M. Bivour, C. Luderer, L. Tutsch, J. Schön, and M. Hermle, “Influence of interfacial oxides at TCO/doped Si thin film contacts on the charge carrier transport of passivating contacts,” *IEEE J PHOTOVOLT*, vol. 10, no. 2, pp. 343–350, 2020.
- [42] J. Haschke, R. Lemerle, B. Aïssa, A. A. Abdallah, M. M. Kivambe, M. Boccard, and C. Ballif, “Annealing of silicon heterojunction solar cells: interplay of solar cell and indium tin oxide properties,” *IEEE J PHOTOVOLT*, vol. 9, no. 5, pp. 1202–1207, 2019.
- [43] M. S. Ashtikar and G. L. Sharma, “Silicide mediated low temperature crystallization of hydrogenated amorphous silicon in contact with aluminum,” *J. Appl. Phys.*, vol. 78, pp. 913–918, 1995.
- [44] A. B. Morales-Vilches, L. Mazzarella, M. Hendrichs, L. Korte, R. Schlatmann, and B. Stannowski, “Nanocrystalline vs. amorphous n-type silicon front surface field layers in silicon heterojunction solar cells: Role of thickness and oxygen content,” in *33rd European Photovoltaic Solar Energy Conference and Exhibition*, Amsterdam, The Netherlands, 2017, pp. 715–719.
- [45] Y. Park, V. Choong, Y. Gao, B. R. Hsieh, C. W. Tang, “Work function of indium tin oxide transparent conductor measured by photoelectron spectroscopy,” *Appl. Phys. Lett.*, vol. 68, no. 19, pp. 2699–2701, 1996.
- [46] S. De Wolf and M. Kondo, “Boron-doped a-Si: H/ c-Si interface passivation: Degradation mechanism,” *Appl. Phys. Lett.*, vol. 91, p. 112109, 2007.
- [47] S. De Wolf, A. Descoedres, Z. C. Holman, and C. Ballif, “High-efficiency silicon heterojunction solar cells: a review,” *Green*, vol. 2, pp. 7–24, 2012.
- [48] Z. C. Holman, A. Descoedres, L. Barraud, F. Z. Fernandez, J. P. Seif, S. De Wolf, and C. Ballif, “Current losses at the front of silicon heterojunction solar cells,” *IEEE J PHOTOVOLT*, vol. 2, pp. 7–15, 2012.
- [49] M. Leilaoui and Z. C. Holman, “Accuracy of expressions for the fill factor of a solar cell in terms of open-circuit voltage and ideality factor,” *J. Appl. Phys.*, vol. 120, p. 123111, 2016.
- [50] D. Pysch, A. Mette, and S. W. Glunz, “A review and comparison of different methods to determine the series resistance of solar cells,” *Sol. Energy Mater. Sol. Cells*, vol. 91, pp. 1698–1706, 2007.
- [51] J.-C. Stang, M.-S. Hendrichs, A. Merkle, R. Peibst, B. Stannowski, L. Korte, and B. Rech, “ITO-free metallization for interdigitated back contact silicon heterojunction solar cells,” *Energy Procedia*, vol. 124, pp. 379–383, 2017.
- [52] Z. C. Holman, M. Filipič, A. Descoedres, S. De Wolf, F. Smole, M. Topič, and C. Ballif, “Infrared light management in high-efficiency silicon heterojunction and rear-passivated solar cells,” *J. Appl. Phys.*, vol. 113, p. 013107, 2013.
- [53] C. Battaglia, A. Cuevas, and S. De Wolf, “High-efficiency crystalline silicon solar cells: status and perspectives,” *Energy Environ. Sci.*, vol. 9, pp. 1552–1576, 2016.
- [54] R. Santbergen, T. Meguro, T. Suezaki, G. Koizumi, K. Yamamoto, and Miro Zeman, “GENPRO4 Optical Model for Solar Cell Simulation and Its Application to Multijunction Solar Cells,” *IEEE J PHOTOVOLT*, vol. 7, no. 3, pp. 919–926, 2017.
- [55] M. R. Vogt, “Development of physical models for the simulation of optical properties of solar cell modules”, PhD Thesis, Technische Informationsbibliothek (TIB), pp.21–42, 2015.
- [56] E. D. Palik, “Handbook of optical constants of solids,” Cambridge, MA, USA: Academic Press, 1985, pp. 355–400.
- [57] S. Duttgupta, F. Ma, B. Hoex, T. Mueller, and A. G. Aberle, “Optimised Antireflection Coatings using Silicon Nitride on Textured Silicon Surfaces based on Measurements and Multidimensional Modelling,” *Energy Procedia*, vol. 15, pp. 78–83, 2012.
- [58] M. A. Green and M. J. Keevers, “Optical properties of intrinsic silicon at 300 K,” *Prog Photovolt Res Appl.*, vol. 3, pp. 189–192, 1995.
- [59] M. A. Green, A. W. Blakers, J. Zhao, A. M. Milne, A. Wang, and X. Dai, “Characterization of 23-percent efficient silicon solar cells,” *IEEE Trans. Electron Devices*, vol. 37, pp. 331–336, 1990.
- [60] J. W. Lathrop, K. Misiakos, and C. W. Davis, “Degradation in silicon solar cells caused by the formation of Schottky barrier contacts during accelerated testing,” in *Proceedings of the 17th IEEE Photovoltaics Specialists Conference*, Kissimmee, FL, USA, 1984, pp. 421–426.
- [61] S. W. Glunz, J. Nekarda, H. Mäckel, and A. Cuevas, “Analyzing back contacts of silicon solar cells by suns-voc-measurements at high

- illumination densities,” in 22nd Eur. Photovolt. Sol. Energy Conf. Exhib., Milan, Italy, 2007, p. 7.
- [62] U. Das, S. Hegedus, L. Zhang, J. Appel, J. Rand, and R. Birkmire, “Investigation of hetero-interface and junction properties in silicon heterojunction solar cells,” in 2010 35th IEEE Photovoltaic Specialists Conference, Honolulu, HI, 2010, pp. 001358–001362.
- [63] S. M. Sze and M. K. Lee, “Carrier transport phenomena; Metal-semiconductor contacts; and Properties of Si and GaAs at 300 K,” in *Semiconductor Devices: Physics and Technology*, 3rd ed. New York, NY, USA: Wiley, 2012, pp. 62, 229–240, 548.
- [64] J. Robertson, “Band offsets, Schottky barrier heights, and their effects on electronic devices,” *J. Vac. Sci. Technol. A*, vol. 31, p. 050821, 2013.
- [65] T. F. Schulze, L. Korte, F. Ruske, and B. Rech, “Band lineup in amorphous/crystalline silicon heterojunctions and the impact of hydrogen microstructure and topological disorder,” *Phys. Rev. B*, vol. 83, p. 165314, 2011.
- [66] P. Procel, G. Yang, O. Isabella, and M. Zeman, “Theoretical evaluation of contact stack for high efficiency IBC-SHJ solar cells,” *Sol. Energy Mater. Sol. Cells*, vol. 186, pp. 66–77, 2018.
- [67] J. M. Shannon and K. J. B. M. Nieuwesteeg, “Tunneling effective mass in hydrogenated amorphous silicon,” *Appl. Phys. Lett.*, vol. 62, pp. 1815–1817, 1993.
- [68] B. J. O’Sullivan, N. H. Thoan, M. Jivanescu, L. Pantisano, T. Bearda, F. Dross, I. Gordon, V. Afanas’ev, A. Stesmans, and J. Poortmans, “Atomic and electrical characterisation of amorphous silicon passivation layers,” *Energy Procedia*, vol. 27, pp. 185–190, 2012.
- [69] O. Nast and S. R. Wenham, “Elucidation of the layer exchange mechanism in the formation of polycrystalline silicon by aluminum-induced crystallization,” *J. Appl. Phys.*, vol. 88, no. 1, pp. 124–132, 2000.